Journal of
Marine Science and Engineering

MDPI

Article

Analysis of the Interannual Variability of Pacific Swell Pools

Xin Zhang [1,2], Kejian Wu [1,2], Rui Li [1,2,3,*], Dongze Li [1,2], Shuai Zhang [4], Ruyan Zhang [5], Shuo Li [3] and Xianghui Dong [1,2]

1 Frontier Science Center for Deep Ocean Multispheres and Earth System (FDOMES) and Physical Oceanography Laboratory, Ocean University of China, Qingdao 266100, China
2 College of Oceanic and Atmospheric Sciences, Ocean University of China, Qingdao 266100, China
3 Department of Infrastructure Engineering, University of Melbourne, Parkville, VIC 3010, Australia
4 Gongyi the Yellow River Yellow River Bureau, Zhengzhou 451200, China
5 Miami College, Henan University, Kaifeng 475001, China
* Correspondence: lirui95@stu.ouc.edu.cn

Abstract: The investigation of the propagation of swells throughout the ocean has long been a subject of significant interest in physical oceanography. This paper investigates the interannual variability of the Pacific swell pools and examines the factors contributing to their formation using the European Centre for Medium-Range Weather Forecasts (ECMWF) ERA5 re-analysis dataset. Our results show that the interaction between swell propagation and wind fields influences the formation and development of Pacific swell pools. The eastern and southern Pacific swell pools are mainly caused by the northward propagation of swells from the South Pacific; the western and northern swell pools are primarily influenced by the southward propagation of swells from the North Pacific; and the central part of the swell pools is the result of the combined impact of both swell propagation from the north and south Pacific. The size of the swell pools in the Pacific Ocean is at its maximum in the northern hemisphere during the winter (December, January, and February) and at its minimum during the summer (June, July, and August). Due to the impact of the low-pressure systems, the swell pools in the winter hemisphere are relatively small, while the swell pools in the summer hemisphere are significantly larger. There is a relationship between the swell pools and ENSO events. When an El Niño event (La Niña event) occurs, the swells propagating to the low latitudes of the Pacific Ocean from high latitudes will strengthen (weaken), resulting in an increase (decrease) in the size of the swell pools. Analyzing the spatial and temporal distribution of the swell pools is important for understanding the large-scale effect of waves.

Keywords: swell pools; swell index; wind fields; ENSO

Citation: Zhang, X.; Wu, K.; Li, R.; Li, D.; Zhang, S.; Zhang, R.; Li, S.; Dong, X. Analysis of the Interannual Variability of Pacific Swell Pools. *J. Mar. Sci. Eng.* **2023**, *11*, 1883. https://doi.org/10.3390/jmse11101883

Academic Editor: Jean-Louis Pinault

Received: 19 August 2023
Revised: 22 September 2023
Accepted: 26 September 2023
Published: 28 September 2023

1. Introduction

Ocean waves are widespread fluctuating phenomena at the ocean surface and significant dynamic processes in the surface layer of the ocean [1]. Wind waves grow and mature due to local winds, and their mean direction aligns with the wind direction [2]. Swells persist on the sea surface even after a sudden change or cessation of the wind, and they travel away from their point of origin to other areas [3,4]. Compared with wind waves, swells have faster speeds of propagation, longer periods, longer wavelengths, and can travel greater distances [5]. According to the studies conducted by Chen et al. [6] and Semedo et al. [7], it has been observed that swells in the ocean are the primary source of energy, and they carry more energy than wind waves.

The study of swell conditions is crucial due to their significant impact on the wave climate of the global oceans. As the importance of swells in air–sea interactions has been recognized, researchers have conducted a series of studies on swells [8–10]. Swells contribute significantly to ocean mixing and are well documented by various studies [7,11–15]. Moreover, swells have detrimental effects on coastal areas. This is particularly critical as coastal regions have high population densities worldwide [16,17]. Potential hazards caused by the swell energy include wave overtopping of sea defenses, significant wave runup, coastal flooding, and inundation. Numerous studies have highlighted the risks posed by swell to coastal areas [14,17]. Given the projected sea level rise and changes in swell climate, beach stability, coastal erosion, nearshore flooding, and the safety of coastal construction and facilities are all at risk. Additionally, it is worth noting that the propagation of ocean swell is a significant source of error in modern spectral wave models, as highlighted by Pathiranas et al. [18]. Swells have immense destructive power in the ocean, posing a potential hazard to ship navigation [19]. After formation, swells exhibit remarkable stability and can be utilized as a reliable source of power generation, offering a more consistent output of electricity at a reduced cost and with significant potential for utilization [20].

Three well-defined swell zones, called swell pools, are located in tropical and subtropical areas [21,22]. Swells play a dominant role in the overall wave composition within the swell pool region [23–25]. Based on empirical formulas and probabilistic statistics of fully grown wind and wave heights in previous studies, three tongue-shaped swell pools are identified in the eastern tropical regions of the Pacific, Atlantic, and Indian Oceans, respectively [21]. However, due to the limitations of inadequate spatial and temporal consistency in the data obtained from a single satellite observation, the analysis of interannual variations in the distribution of a swell has not been conducted. Using the ERA-Interim wave re-analysis data from the European Centre for Medium-Range Weather Forecasts (ECMWF), Deng et al. [26] made enhancements to the swell index algorithm developed by Chen et al. [6]. Deng et al. [26] identified the presence of a swell pool in the eastern Pacific Ocean and examined the amount of water transported in this pool. The study suggested that the water transport of the swell could potentially influence oceanic circulation [26]. Instead of using multi-year time-series statistics, the method calculates the probability of swell occurrence monthly [26]. This new approach allows for a more accurate calculation of the swell index for each month of the year, taking into account the changing probability of swell events throughout the year [27,28]. Afterward, researchers utilized the ERA-Interim wave re-analysis data and the swell calculation method developed by Chen [6] to examine the climatic characteristics of swells in the northern Indian Ocean. They pointed out that the swell energy transmitted from the southern hemisphere to the Indian Ocean is enormous before and after the monsoon.

Based on the previous calculation method of the swell index, Zheng et al. [29] introduced a novel approach for calculating the swell index using energy flow density. This new method yields a larger area for the swell pools compared to the previous results. Li [30] discovered four more significant cross-swell pools. Liu and Zhao [31] used numerical modeling to point out that swell pools originate from both the northern and southern hemispheres, move towards the south, and divide into two separate pools during the winter.

Understanding the swell pool formation and variability mechanisms could potentially inform decision-making related to ocean navigation and maritime safety in the Pacific Ocean; by understanding how swells propagate, and the formation and variation of swell pools, researchers and maritime authorities can gain insights into the behavior and characteristics of these oceanic phenomena. This knowledge can be used to develop more accurate swell forecasts, which can help mariners and navigators make informed decisions regarding route planning, vessel operations, and safety measures. Additionally, understanding the impact of swells on swell pools can contribute to the identification of potential hazards or areas of increased risk, allowing for appropriate precautions to be taken to ensure maritime safety in the Pacific Ocean.

The current investigation on the swell pools in the Pacific Ocean remains unfinished, and there is still a lack of understanding of the cause and interannual variations of the swell pools [31]. This paper aims to elucidate the causes of the Pacific Ocean swell pools and their interannual variability and offers novel perspectives and valuable insights for further research on swell pools and their relationship with the ocean climate. The paper is structured as follows: Section 2 describes the ERA5 re-analysis data used in this study and how the swell index is calculated; Section 3 investigates the global distribution of wave fields and the causes of swell pool formation, including the propagation of swells and the effects of wind fields; Section 4 examines and analyzes the interannual variations of the swell pools, including the relationship with ENSO; and Section 5 offers our concluding remarks and summary.

2. Data Sources and Research Methodology

2.1. Data

The dataset used in this paper is derived from ERA5, a fifth-generation re-analysis dataset provided by the European Centre for Medium-Range Weather Forecasts (ECMWF). The ocean wave parameters in ERA5 are derived from a fully coupled atmosphere–wave model called WAM, which utilizes satellite radar altimeter data to determine wave height [32]. The errors of the ERA5 dataset mainly come from the error of observed data and the error of model simulation [33]. Although there are minor errors, extensive research has demonstrated the reliability of ERA5 data [34–36]. The ocean wave data of ERA5 were also validated by WAVEWATCH III model data and buoy data by Liu et al. [37] and Rascle et al. [38]. The calculation method of wave parameters is described in the official IFS documentation Part VII: ECMWF wave model (https://www.ecmwf.int/sites/default/files/elibrary/2023/81373-ifs-documentation-cy48r1-part-vii-ecmwf-wave-model.pdf, accessed on 1 September 2023). ERA5 can be considered as a globally harmonized dataset. In this study, we utilized data from 1979–2020 to analyze the significant wave height, mean wave period, mean wave direction, wind speed, and wind direction of total waves, wind waves, and swells. The data were collected on a monthly basis and had a spatial resolution of $0.5° \times 0.5°$ for waves and $0.25° \times 0.25°$ for wind fields. This spatial and temporal resolution level was chosen to ensure that it met the requirements for studying the interannual variability and genesis of the Pacific swell pools.

2.2. Method

When calculating the swell index, Chen et al. [6] first judged whether the wave was a swell and considered the probability of the swell. Then, the swell index was obtained by calculating the proportion of wind wave energy. The wave energy can be calculated by $E \approx \frac{\rho g^2}{64\pi} T H^2$, where T is the wave period and H is the significant wave height. The ERA5 dataset offers the parameters of wind waves and swells separately. So, the wind wave energy and swell energy can be calculated, respectively. The method employed in this paper is the enhanced swell index method developed by Zheng [29]. This method computes the swell index using the significant wave height and the mean wave period, utilizing the following formula:

$$S = \frac{E_S}{E_T} \propto \frac{{H_S}^2 T_S}{{H_T}^2 T_T} \tag{1}$$

where S is the swell index, E_S is the swell energy, E_T is the mixing energy (total wave energy), H_S is the significant wave height of the swell, T_S is the mean period of the swell, H_T is the significant wave height of the mixing wave, and T_T is the mean period of the mixing wave. In this context, we classify the region as a swell pool when the value of S is greater than 0.9. A higher value of S indicates a stronger influence of swells in the overall makeup of the waves in that particular area.

3. The Causes of Swell Pools

3.1. Global Distribution of Swell Indexes

Before studying the spatial distribution of swell pools, it is important to understand the spatial distribution of wind waves, swells, and total waves. By examining Figure 1, it is evident that swells generally have significantly larger wave heights and periods compared to wind waves. Upon comparing Figure 1a,c, and e, we find that the spatial distribution of total wave periods is similar to the swells, with extreme areas concentrated in the westerly zone and equatorial region of the southern hemisphere. Analyzing Figure 1b,d,f further reveals that the highest significant wave heights of wind waves, swells, and total waves are all situated in the westerly zone of the southern hemisphere. This indicates that waves in this region have the opportunity to develop and propagate, creating favorable conditions for northward waves in the southern hemisphere.

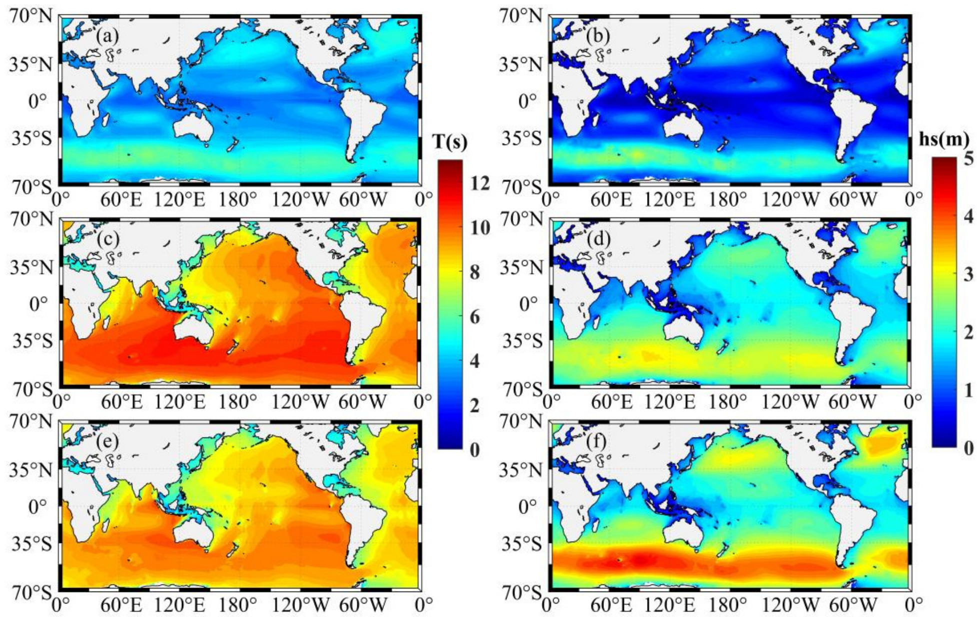

Figure 1. Distribution of monthly average wave period and significant wave height calculated from 1979–2020. Wind wave period (**a**); wind wave height (**b**); swell period (**c**); swell height (**d**); total wave period (**e**); and total wave height (**f**). T (s) is the period, and hs (m) is the significant wave height.

To study the factors that contribute to the formation of swell pools further, it is essential to have a clear understanding of their spatial distribution. A better understanding of seasonal variation in swell pools will allow appropriate actions to mitigate potential risks and plan the construction of coastal structures, offshore activities, and shipping routes [39]. Swells play a vital role in transferring momentum, heat, and energy between the atmosphere and the ocean at the air–sea boundary. The study of seasonal variations in swell pools is also an important contribution to understanding ocean climate in low-latitude oceans. Figure 2 shows that swell pools are predominantly found between 30° north-south latitudes. Additionally, the size of these swell pools increases as one reaches closer to the equator. These swell pools are distributed across the Pacific, Atlantic, and Indian Oceans. It is worth noting that no swell pools are observed at high latitudes. The swell pools exhibit a distribution pattern along zonal bands, with noticeable changes in characteristics throughout the seasons. Due to the presence of a low-pressure system in the winter hemisphere, the powerful winds will generate increased wind waves and result in a greater number of swells moving across the equator and into the summer hemisphere. Consequently, this will ultimately lead to the formation of larger swell pools in the summer hemisphere.

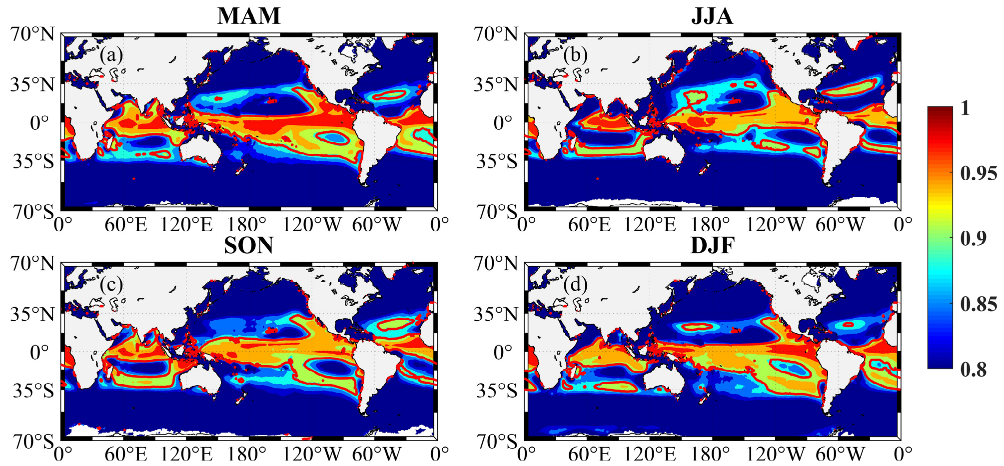

Figure 2. Distribution of the global swell index averaged over 1979–2020. The swell pools are shown in the red line areas (S > 0.9). ((**a**) MAM: March, April, and May; (**b**) JJA: June, July, and August; (**c**) SON: September, October, and November; (**d**) DJF: December, January, and February).

3.2. Effect of Wave Propagation on the Swell Pools

Many studies have examined the propagation paths of Pacific Ocean swells [18,40]. According to the propagation direction of the South Pacific Ocean swells, we analyzed the variation of abnormal swell height signals along the path of swell propagation from high to low latitudes, as shown in Figure 3a,b. The starting point is at (57° S, 150° W) and an ending point at (12° S, 105° W), going through the point (35° S, 128° W). The abnormal signals originating from the Southern Ocean wave field gradually weaken during the process of northward propagation. When El Niño occurs, an unusually strong northward swell originating in the Southern Ocean can be clearly observed, for example, in 1998, as shown in Figure 3c. In contrast, when La Niña occurs, the northward swell is weakened, for example, in 1989, as shown in Figure 3d.

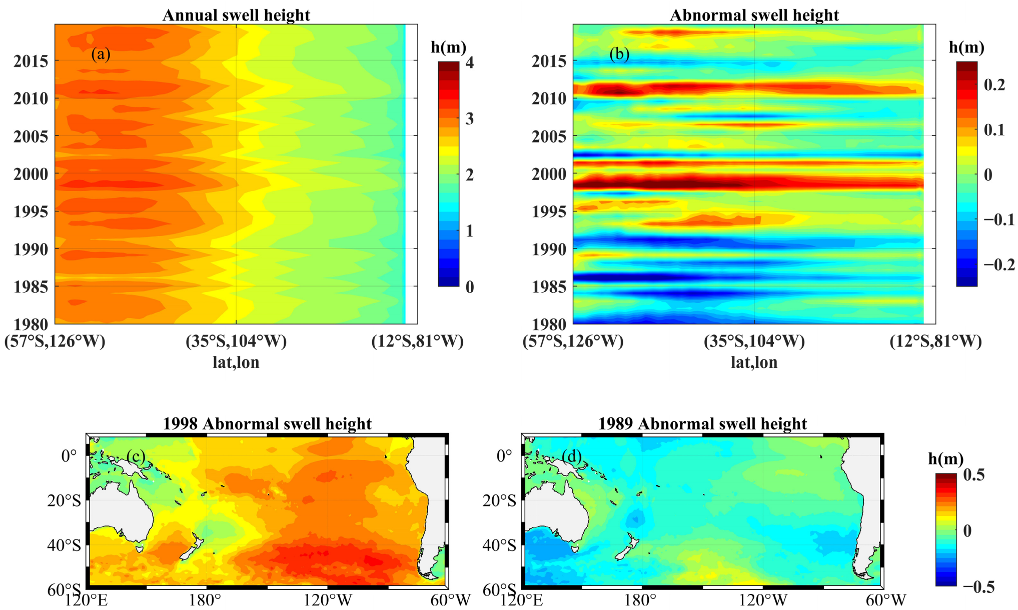

Figure 3. The annual swell height (**a**) and abnormal annual swell height (**b**) (detrended annual mean) from (57° S, 150° W) to (12° S, 105° W). The spatial distribution of the abnormal swell height in 1998 (**c**) and 1989 (**d**).

The correlation coefficients are analyzed between the total wave heights along the 50° N latitude in the North Pacific or 50° S in the South Pacific and the Pacific swell heights. In our study, we focus on four specific points on each latitude line to represent the overall spatial characteristics of these regions.

Figure 4 shows a strong correlation between the total waves in the South Pacific along the 50° S latitude and the eastern and southern Pacific swell pools. Besides the area around the selection point, high correlation coefficients are also observed for the 20° S latitude and the Peru–Chile coast. With the selection points moving eastward, the extreme regions of the correlation coefficients also move eastward. By comparing Figure 2, we can observe that the coastal region of Peru–Chile consistently experiences high levels of swell indexes throughout the year, which belongs to the range of swell pools. When we consider Figure 4 in conjunction with this, it becomes reasonable to assume that the waves originating from the South Pacific Ocean become obstructed by the topography of South America when they reach the Peru–Chile coast. As a result, these waves accumulate in this particular area, leading to the formation of swell pools. It is worth noting that the strong correlation coefficient from the South Pacific extends across the equator to 20° N in the Eastern Ocean.

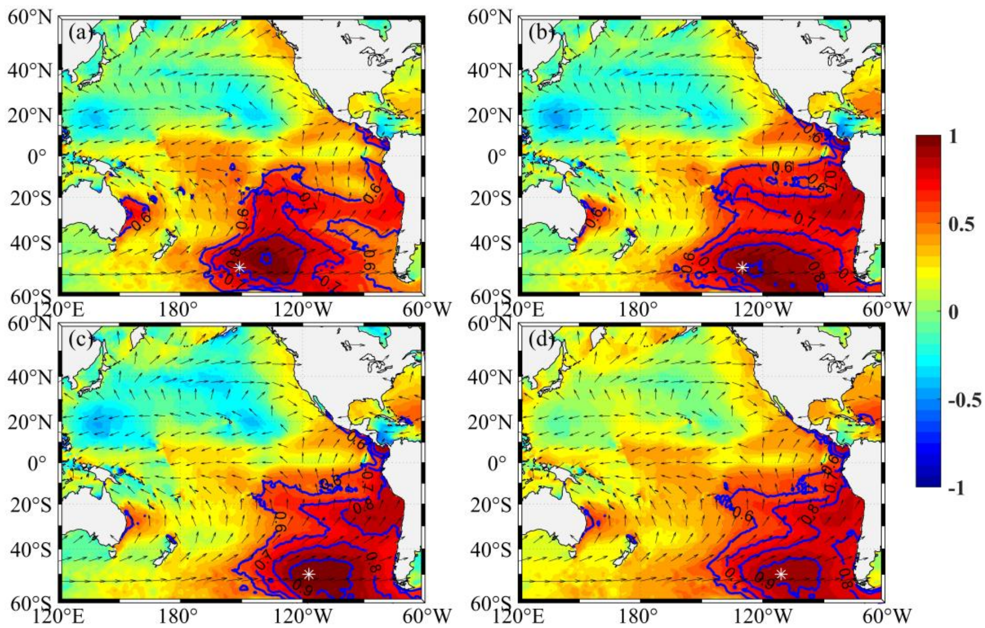

Figure 4. Spatial distribution of correlation coefficients between monthly total significant wave heights at 50° S latitude and significant swell heights in the Pacific ((**a**) 151° W; (**b**) 130° W; (**c**) 117° W; and (**d**) 111° W), calculated from 1979 to 2020. The direction of the arrow indicates the mean swell direction.

Carrasco [41] proposed that northward propagating swells in the Southern Hemisphere originate in the Southern Ocean. As depicted in Figure 4, it is evident that waves originating from the South Pacific Ocean have the ability to traverse the eastern section of the Pacific Ocean and cross the equator to reach the Northern Hemisphere. However, these waves are unable to propagate through the western part of the Pacific Ocean to reach the Northern Hemisphere. The reason behind this limitation may lie in the intricate topography and the presence of numerous islands in the western Pacific Ocean, which hinder the propagation of waves. Consequently, this is also the explanation for why the area with high correlation coefficients in the South Pacific can extend northward along the Eastern Ocean to the low-latitude region of the North Pacific but fails to extend northward along the Western Ocean. Furthermore, it can be observed that there is a notable concentration of strong correlation coefficients along the 20° S latitude, specifically in the eastern and southern sections of the average swell pools. This suggests that the propagation of waves from the South Pacific region has an impact on the eastern and southern areas of the swell pools.

Combining the areas of high values of the correlation coefficients and the direction of propagation of the swells, it can be seen that the eastern and southern regions of the Pacific swell pools are the result of the northward propagation of waves from the South Pacific Ocean.

Figure 5 shows that the total waves at the 50° N latitude in the North Pacific Ocean are closely related to the eastern and northern Pacific swell pools. Furthermore, the region exhibiting the highest correlation coefficient is observed to move in a westerly direction as the chosen points move further toward the west. It is also evident that the North Pacific waves propagate along the southern direction to the lower latitude ocean. In addition, we have observed a high correlation coefficient in the low-latitude South Pacific Ocean. This may be the result of waves from the North Pacific Ocean propagating across the equator to the Southern Hemisphere. By considering the direction of wave propagation and the high correlation coefficients, we can conclude that the western and northern Pacific Ocean swell pools are formed due to the southward propagation of waves from the North Pacific Ocean.

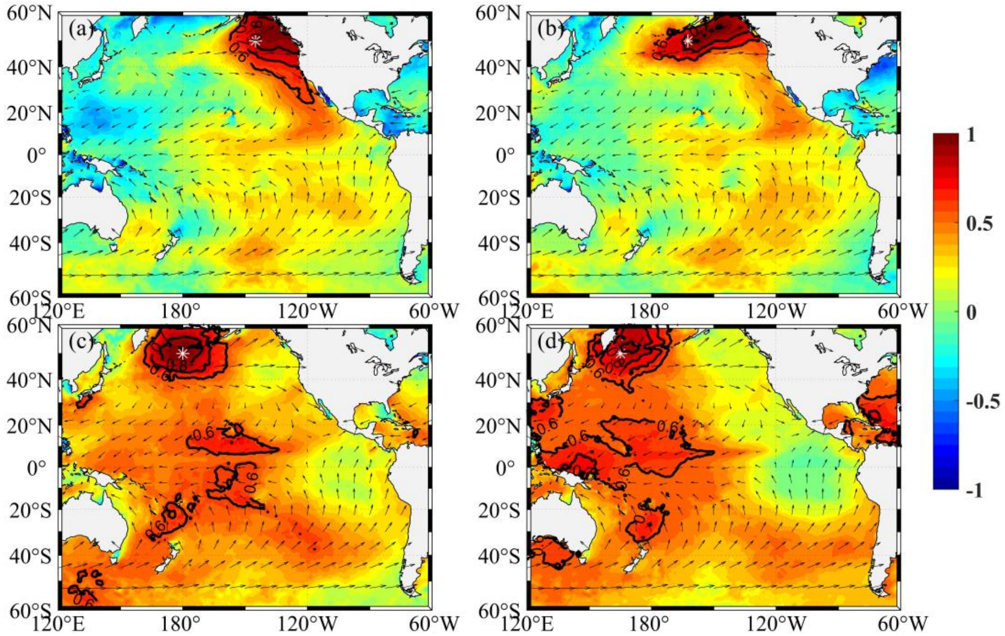

Figure 5. Same as Figure 4 but for total significant wave heights at 50° N latitude and significant swell heights in the Pacific ((**a**) 145° W; (**b**) 162.5° W; (**c**) 180° W; and (**d**) 165° E).

Comparing Figures 4 and 5, the western and northern equatorial Pacific swell pools are primarily created by the southward propagation of total waves from the North Pacific. On the other hand, the swell pools in the eastern and southern equatorial Pacific are primarily formed by the northward propagation of total waves from the South Pacific. The correlation coefficient between the swell pools at the junction of the high values of the two figures with the North and South Pacific Oceans is not high. This suggests that the swell pools in the equatorial Pacific Ocean are likely formed by the combined waves originating from the North and South Pacific Ocean.

The phenomenon of wave propagation in both the northern and southern hemispheres crossing the equator can help explain why the size of swell pools in the same hemisphere is larger in the summer compared to the winter. When the hemisphere is in winter, the wind field is stronger, allowing waves to spread to a more distant area and cross the equator. So, the accumulation of waves in the low-latitude wave is decreased, resulting in smaller swell pools. On the contrary, when the hemisphere is in summer, the wind field is weaker, the waves travel short distances, and more waves remain in the hemisphere, resulting in larger swell pools in that hemispheric region.

The EOF analysis method is commonly used in the analysis of large-scale climatic data, playing a crucial role in capturing spatial and temporal characteristics [42,43]. In Figures 6 and 7, we apply the EOF method to examine the Pacific swell and total waves, respectively. This analysis helps us determine the spatial distributions of the first two EOFs (EOF1 and EOF2). The variance contribution of the main mode of the Pacific Ocean swell EOF1 is 40.3%. The spatial distribution pattern of EOF1 indicates that the swell is propagating northward away from its formation region in the Southern Ocean. The spatial distribution is dominated by negative anomalies, with one negative anomaly center in the North and South Pacific Oceans. On the other hand, the spatial distribution of EOF2 is dominated by a north–south antiphase distribution, with negative anomaly centers dominating in the North Pacific Ocean and positive anomaly centers dominating in the South Pacific Ocean.

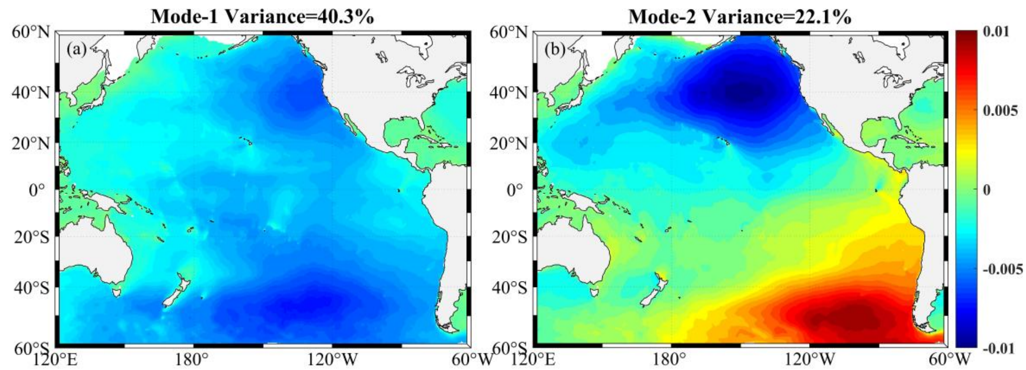

Figure 6. The spatial pattern of the empirical orthogonal functions (EOF) of significant swell height (detrended monthly average) in the Pacific Ocean for 1979–2020: (**a**) EOF1 and (**b**) EOF2.

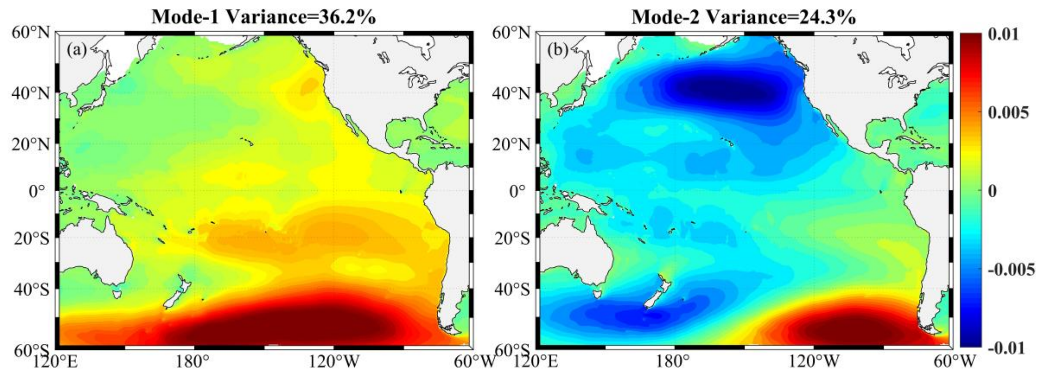

Figure 7. The spatial pattern of the empirical orthogonal functions (EOF) of total significant wave height (detrended monthly average) in the Pacific Ocean for 1979–2020: (**a**) EOF1 and (**b**) EOF2.

The EOF main mode (EOF1) of total wave height contributes 36.2% to the variance. In Figure 7a, the spatial distribution is primarily characterized by positive anomalies. The center of the anomalies is located in the Southern Ocean and is mainly influenced by the low-pressure systems. The spatial distribution of the total wave EOF2 is similar to that of the swell EOF2. It exhibits a north–south antiphase distribution, with both positive and negative anomalies gradually diminishing towards the equator. This observation further supports the idea that swells from the North and South Pacific Ocean propagate towards the equatorial region.

3.3. Effects of Wind Fields on the Swell Pools

As shown in Figure 8, it can be observed that areas where swell pools form have relatively weaker wind, while regions with higher wind strength, such as the westerly wind zone, do not support the formation of swell pools. This means that the formation and development of swell pools are not only related to wave propagation but also affected by the local wind field. The seasonal variation of swell pools is obvious. During the winter in the northern hemisphere, the global swell pool area is considerably larger compared to the summer in the northern hemisphere. Comparisons indicate that during winter, the overall strength of the global wind field is lower than in summer, which is more favorable for the formation of swell pools. In the western part of South America, there is a noticeable indentation in the swell pool, and during the middle of summer, this indentation expands along the zonal axis and decreases the swell pool due to the influence of strong wind fields. It is logical to propose that the formation of the swell pool can be attributed to the relatively weaker local wind field, which leads to lower wind wave intensities. As a result, the swell develops sufficiently, establishing a dominant presence in the wave field and ultimately resulting in the formation of the swell pools. By analyzing the wind speed distribution in relation to the spatial distribution of the swell indexes in Figure 8, it is evident that the boundary of the swell pool aligns closely with the 6 m/s wind speed. The contour of the 6 m/s sea surface wind speed and the boundary of the swell pools exhibit a link across all seasons. When the wind speed is less than 6 m/s, the wind wave intensity in the area is low, allowing the swells to spread out and build up, which is advantageous for forming a swell pool. On the other hand, when the wind speed exceeds 6 m/s, the wind strength in the area becomes too strong, hindering the accumulation of swells and preventing the formation of a swell pool. Consequently, wind speed plays a significant role in the formation and transformation of swell pools.

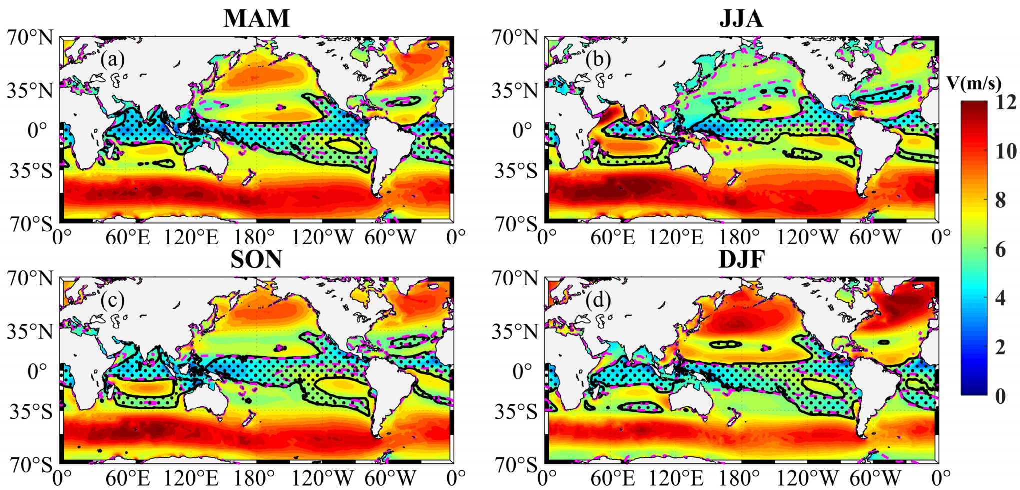

Figure 8. Seasonal spatial distribution of sea surface 10 m high wind speeds. The purple dashed line is the 6 m/s sea surface wind speed contour. The black boxed line is the swell pool's boundary. The scattered areas are the swell pools. (MAM (**a**): March, April and May; JJA (**b**): June, July and August; SON (**c**): September, October and November; DJF (**d**): December, January and February).

4. The Annual Variability of the Swell Pools

4.1. Northward Swells in the Global Ocean

As can be seen from Figures 2 and 8, the swell pools are characterized by obvious seasonal variations. Since the formation of swell pools and the meridional propagation of swells have a link, studying the distribution of swells in the meridional direction holds great significance. As shown in Figure 9, it is evident that there is a consistent northward propagation of swells in the South Pacific Ocean, from 40° S to the equatorial region. Conversely, there is an overall southward movement of swells in the North Pacific Ocean.

The northward swells in the South Pacific display noticeable seasonal variations. During summer, the northward swell is at its highest, while during winter, it is at its lowest. This can be attributed partly to the northward and southward shifts of the equatorial trade wind belt, influenced by the change in the position of the subsolar point, which impacts the northward swell across the equator. Additionally, the weaker wind field in the summer hemisphere restricts the spread of the swell, whereas the stronger wind field in the winter hemisphere allows for sufficient propagation of the swell. The observation that northward swells in the South Pacific can reach as far as 20° N across the equator suggests that swells originating in the westerly belt areas of the Southern Hemisphere possess significant energy in their northward propagation.

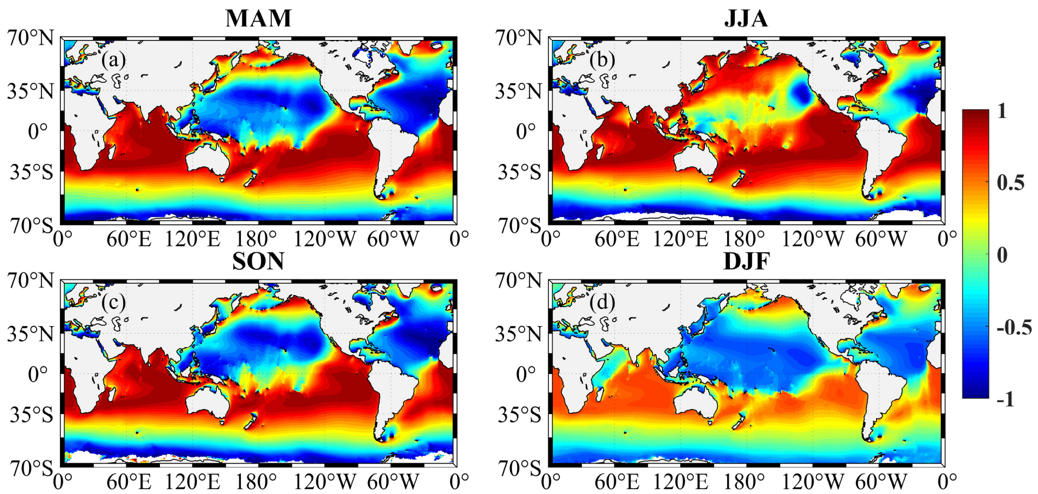

Figure 9. Spatial distribution of the global northward swell. Values of 1 indicate a northward direction, while values of −1 indicate a southward direction. (MAM (**a**): March, April and May; JJA (**b**): June, July and August; SON (**c**): September, October and November; DJF (**d**): December, January and February).

Figure 10a,b display the time series of the abnormal northward swell area proportion in the North and South Pacific Ocean over 42 years. The magnitude of the value reflects the intensity of the northward swell anomaly. The figure reveals a relationship between ENSO events and the northward swell area proportion in both the North and South Pacific regions. It is important to note that El Niño events of varying intensities have distinct impacts on the proportion of southward swells in the North Pacific. During instances of strong El Niño events, such as in 1982, 1997, and 2016, there was a more noticeable increase in the proportion of southward swells in the North Pacific. Conversely, when strong La Niña events occurred, the decrease in the proportion of equatorward swells in the Pacific was insignificant. This indicates a relationship between El Niño events and the increase of equatorward swells in the Pacific.

There exists a significant relationship between the swell pools and ENSO events. It is important to note that El Niño events have a greater impact on the anomalies in the regions of northward swell in the Pacific. This impact is more pronounced compared to the strengthening of the atmospheric circulation system caused by El Niño. On the other hand, the impact of La Niña events is relatively small and more difficult to detect, especially after the weakening of the seasonal variability signal. The variability of the swell pools is affected by not only the total waves in the Pacific Ocean but also the ENSO events, making the factors influencing this change complex.

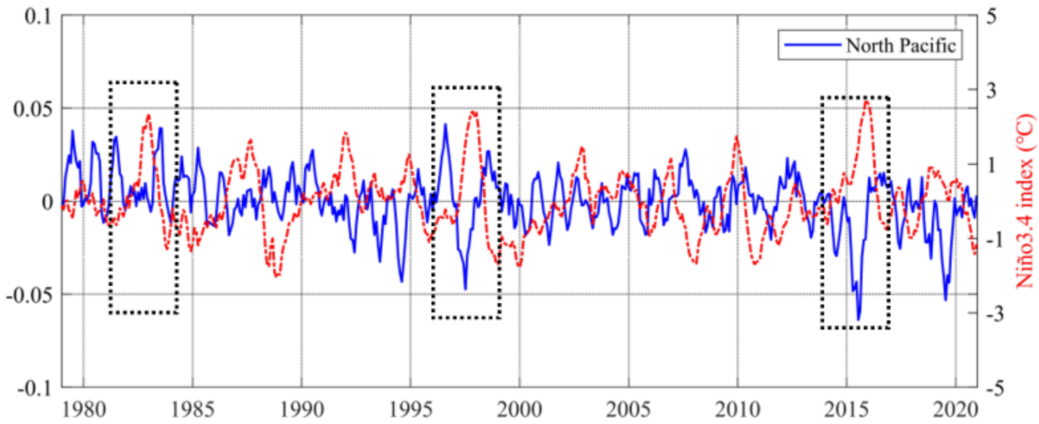

(**a**)

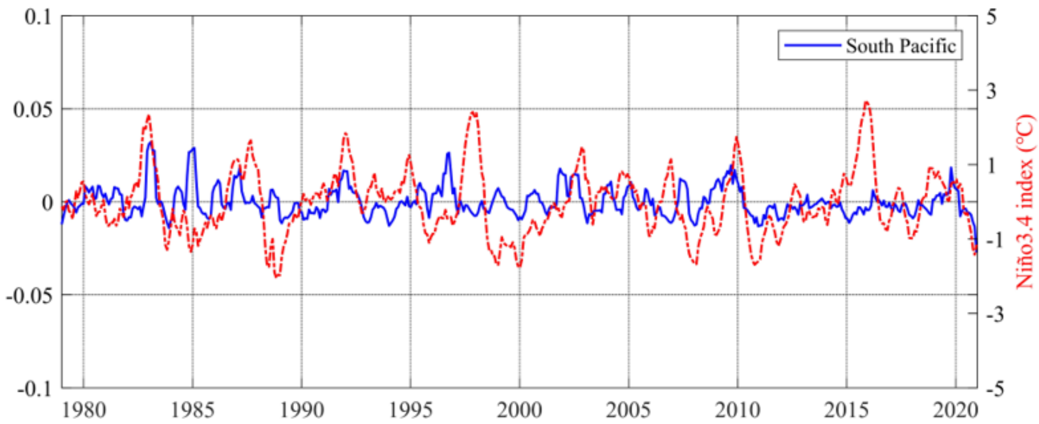

(**b**)

Figure 10. (**a**) Time series of the ratio of the number of grids of the northward swells to the total number of grids in the North Pacific (10° N–50° N); (**b**) same as (**a**) but for the South Pacific (10° S–50° S). The red dashed line represents the Niño 3.4 index.

4.2. Case Study

To better understand the impact of ENSO on the swell pools, we specifically analyzed the strongest El Niño year (1997–1998) and the strongest La Niña year (1988–1989). Figure 11 illustrates that the swell pool area is largest during winter and smallest during summer. Compared to the average swell pool distribution over the 42 years, the intensity and extent of the swell pools during all seasons of the El Niño year are greater than shown in Figure 2. It is evident that the El Niño event has a particularly significant impact in the equatorial region, with a mean swell index greater than 0.95. In addition, it should be noted that the swell pools along the 30° latitude are still seasonal and have increased in size considerably. It is important to highlight that during summer, the area and intensity of 30° N swell pools significantly increase. Conversely, during winter, the area and intensity of 30° S swell pools experience a significant increase. This leads us to hypothesize that in the summer hemisphere, low-latitude wind and wave intensity are low while swell intensity is high, which favors the formation of swell pools. In conclusion, the occurrence of the El Niño phenomenon affects the changes in the area of the swell pools.

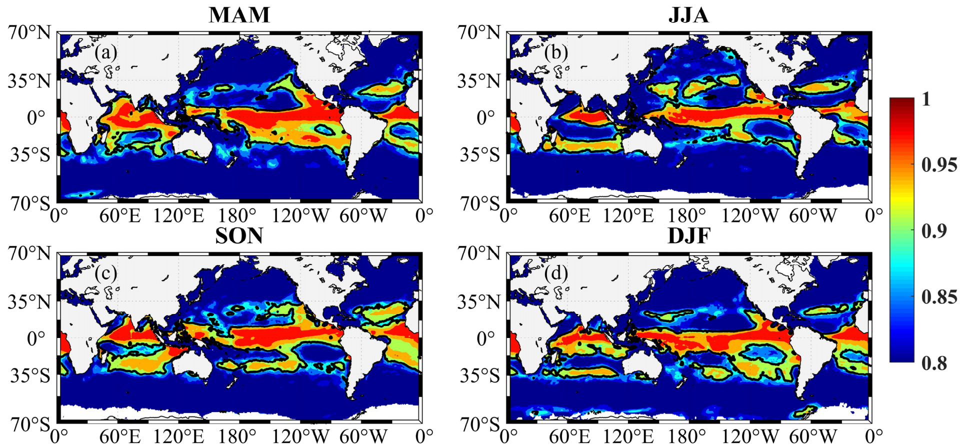

Figure 11. Distribution of global swell index in strong El Niño event (1997–1998). The Niño 3.4 index is 0.50 °C. The areas surrounded by the black line are the swell pools (S > 0.9). (MAM (**a**): March, April and May; JJA (**b**): June, July and August; SON (**c**): September, October and November; DJF (**d**): December, January and February).

During the 42-year from 1979 to 2020, the strongest La Niña event happened in 1988. Therefore, studying the impact of La Niña events on the swell pools can be better accomplished by analyzing the spatial distribution of swell indexes for that specific year. During La Niña years, swell indexes were consistently low throughout the year, leading to a contraction in the size of the swell pools. Generally, the swell pools were smaller in the summer and fall seasons and larger in the winter and spring seasons. By comparing Figures 2c and 12c, it is evident that the equatorial Pacific swell pools were significantly reduced during the fall of La Niña, specifically from September to November. The seasonal characteristics of the swell pools remained consistent, with the largest pool occurring in winter and the smallest pool in summer. In conclusion, the La Niña event did not favor the formation of swell pools.

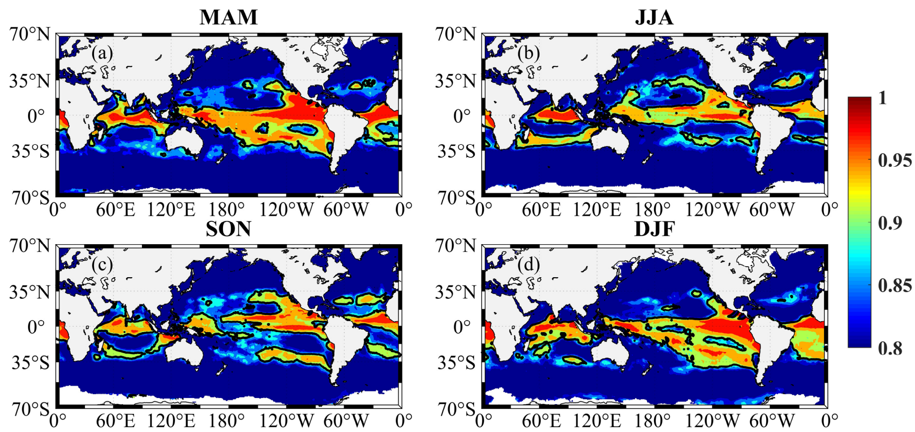

Figure 12. Same as Figure 11, but for a strong La Niña event (1988–1989). The Niño 3.4 index is −0.90 °C. (MAM (**a**): March, April and May; JJA (**b**): June, July and August; SON (**c**): September, October and November; DJF (**d**): December, January and February).

The El Niño events will strengthen the atmospheric circulation system. Therefore, the El Niño events enhance the propagation of waves from the South and North Pacific towards the equator by strengthening the atmospheric circulation system. This leads to waves reaching lower latitudes, crossing the equator, and traveling to further locations. Consequently, the change in the proportion of northward total swells during the occurrence of the El Niño event becomes more significant. Similarly, during La Niña, the change in the proportion of northward total swells becomes smaller because of the abnormal cooling in the Pacific equatorial region, which weakens the atmospheric circulation system. As a result, the swells traveling to lower latitudes in the hemisphere during winter are weakened. Ultimately, this leads to a smaller change in the proportion of northward total swells during La Niña.

5. Summary

Swell pools are primarily found in the Pacific Ocean, Indian Ocean, and Atlantic Ocean, concentrated in the region between 30° north and south latitude. This study specifically examined the causes and variations of swell pools in the Pacific Ocean. The Pacific Ocean swell pools exhibit distinct seasonal variations, with the largest area occurring in winter and the smallest in summer. In the winter hemisphere, the swell propagates longer distances meridionally and can even cross the equator. Furthermore, the winter hemisphere experiences stronger wind waves, causing the size of the swell pools in the Pacific Ocean to decrease in that hemisphere. On the other hand, the summer hemisphere has weaker wind waves, which leads to an increase in the size of the swell pool in the Pacific Ocean in that hemisphere. There are notable distinctions in the behavior of swell pools in the eastern and southern Pacific regions compared to those in the western and northern regions. Firstly, the direction of the swells varies between these two areas. The eastern and southern Pacific swell pools are primarily influenced by northward swells, whereas the western swell pool experiences predominantly westward swells. Secondly, there is a discrepancy in size between the eastern and western swell pools, with the eastern swell pools being larger than the western swell pools.

The formation and variation of Pacific swell pools are connected to the propagation of waves in the North and South Pacific. Some of the waves originating from mid-to-high latitudes will leave the wind field and travel as swells toward lower latitudes. These swells become the dominant force in the waves when they reach the breezy low-latitude oceans. Depending on the direction of the swell's propagation, swells from the Northern Hemisphere mainly travel towards the Western Pacific Ocean, while swells from the Southern Hemisphere mainly travel towards the Eastern Pacific Ocean. Thus, the formation of the eastern and southern Pacific Ocean swell pools results from the northward propagation of South Pacific waves; the formation of the western and northern Pacific Ocean swell pools results from the southward propagation of North Pacific waves. Meanwhile, in the equatorial region of the Pacific Ocean, swell pools are formed by the combined effect of waves from both the North and South Pacific.

The formation and variation of the swell pools are related to the wind field. There is a significant overlap between the boundary of the swell pools and the contour representing wind speeds of 6 m/s. When the wind speed is less than 6 m/s, the strength of the wind waves in the area is low, which promotes the development of swell pools. Conversely, when the wind speed exceeds 6 m/s, the wind intensity in the region becomes too strong for swell pools to form.

There is a clear link between the intensity of ENSO events and variations in swell pools. During an El Niño event, the global range of swell pools expands, significantly increasing the swell index. El Niño events facilitate the creation of swell pools. Conversely, the occurrence of a La Niña event hinders the formation of swell pools. Therefore, the size of the swell pools will keep increasing in the future if there are more El Niño events and will decrease if there are more La Niña events. Swell pools are important for transporting and accumulating nutrients, phytoplankton, and other marine organisms. Changes in their size can disrupt the natural flow of these resources, leading to altered marine productivity and food availability for marine organisms. Swell pools play a role in shaping coastlines and influencing sediment transport. Any alterations in their size can impact coastal erosion patterns, sediment dynamics, and beach nourishment processes. This, in turn, can affect the stability of coastal landforms and impact coastal communities and infrastructure.

Young et al. [44] have observed a global increase in significant wave heights, particularly in the Southern Ocean. Increased swell from the Southern Ocean and increased size of the swell pools. Therefore, in the long-term future, the size of the swell pools may continue to expand. Currently, there is a growing interest in exploring the relationship between large-scale wave effects and climate phenomena. This paper aims to contribute valuable insights to this field of research. Specifically, it focuses on studying the reasons and patterns of change in swell pools within the Pacific Ocean. However, it lacks a comparative analysis of swell pools in the Indian and Atlantic Oceans. Furthermore, this paper relies on the ERA5 dataset for analysis, which has limitations in terms of data variety. It is recommended that more reliable data be used to validate the accuracy of the results.

Author Contributions: Conceptualization, X.Z. and R.L.; formal analysis, K.W.; funding acquisition, K.W.; investigation, S.Z.; methodology, S.Z.; project administration, R.L.; resources, K.W.; validation, K.W. and X.Z.; Visualization, R.L. and S.L.; writing—original draft, X.Z. and R.Z.; writing—review and editing, D.L., X.Z. and X.D. and R.L. All authors have read and agreed to the published version of the manuscript.

Funding: This research was funded by the National Natural Science Foundation of China under grant number 42176018.

Data Availability Statement: The data used in this study are all provided by the European Centre for Medium-Range Weather Forecasts (ECMWF) (https://cds.climate.copernicus.eu/cdsapp#!/dataset/reanalysisera5-single-levelsmonthly-means?tab=form, accessed on 1 September 2023).

Acknowledgments: The authors thank the researchers who obtained and published the data and schemes used in this study. R.L. acknowledges the fellowship provided by the China Scholarship Council (CSC:202206330001).

Conflicts of Interest: The authors declare that the research was conducted in the absence of any commercial or financial relationships that could be construed as potential conflicts of interest.

References

1. James, W. Effects of plane progressive irrotational waves on thermal boundary layers. *J. Fluid Mech.* **1971**, *50*, 321–334.
2. Jesús, P. The global signature of ocean wave spectra. *Geophys. Res. Lett.* **2017**, *45*, 267–276.
3. Polyakova, A.M.; Sugak, S.S. Wind waves and swell in the north pacific. *Russ. Meteorol. Hydro.* **2004**, 61–67.
4. Barnett, T.P. Wind waves and swell in the North Sea. *Eos Trans. Am. Geophys. Union* **1970**, *51*, 544–550. [CrossRef]
5. Shi, Y.F.; Yang, Y.Z.; Wu, K.J.; Sun, B.N. The signal of La NiÃ±a in wave transport. *Int. J. Appl. Earth Obs.* **2018**, *70*, 118–124.
6. Chen, G.; Chapron, B.; Ezraty, R.; Vandemark, D. A global view of swell and wind sea climate in the ocean by satellite altimeter and scatterometer. *J. Atmos. Ocean. Technol.* **2002**, *19*, 1849–1859. [CrossRef]
7. Semedo, A.; Sušelj, K.; Rutgersson, A.; Sterl, A. A Global View on the Wind Sea and Swell Climate and Variability from ERA-40. *J. Clim.* **2011**, *24*, 1461–1479. [CrossRef]
8. Liu, J.; Meucci, A.; Young, I.R. Projected wave climate of Bass Strait and south-east Australia by the end of the twenty-first century. *Clim. Dynam.* **2023**, *60*, 393–407. [CrossRef]
9. Jin, L.; Alberto, M.; Qingxiang, L.; Babanin, A.V.; Daniel, I.; Young, I.R. The wave climate of Bass Strait and South-East Australia. *Ocean Model.* **2022**, *172*, 101980.
10. Liu, B.; Wu, K.J.; Guan, C. Global Estimates of Wind Energy Input to Subinertial Motions in the Ekman-Stokes Layer. *J. Oceanogr.* **2007**, *63*, 457–466. [CrossRef]
11. Högström, U.; Rutgersson, A.; Sahlée, E.; Smedman, A.; Hristov, T.S.; Drennan, W.M.; Kahma, K.K. Air-sea interaction features in the baltic sea and at a pacific Trade-Wind site: An inter-comparison study. *Bound.-Lay. Meteorol.* **2013**, *147*, 139–163. [CrossRef]
12. Cavaleri, L.; Fox-Kemper, B.; Hemer, M. Wind waves in the coupled climate system. *Bull. Am. Meteorol. Soc.* **2012**, *93*, 651–661. [CrossRef]
13. Högström, U.; Smedman, A.S.; Semedo, A.; Rutgersson, A. Comments on 'A Global Climatology of Wind-Wave Interaction'. *Am. Meteorol. Soc.* **2011**, *41*, 1811–1813. [CrossRef]
14. Ardhuin, F.; Chapron, B.; Collard, F. Observation of swell dissipation across oceans. *Geophys. Res. Lett.* **2009**, *36*, 391–400. [CrossRef]
15. Fairall, C.W.; Bradley, E.F.; Hare, J.E.; Grachev, A.A.; Edson, J.B. Bulk parameterization of air-sea fluxes: Updates and verification for the COARE algorithm. *Am. Meteorol. Soc.* **2003**, *16*, 571–591. [CrossRef]
16. Li, R.; Wu, K.; Zhang, W.; Dong, X.; Lv, L.; Li, S.; Liu, J.; Babanin, A.V. Analysis of the 20-Year variability of ocean wave hazards in the northwest pacific. *Remote Sens.* **2023**, *15*, 2768. [CrossRef]

17. Amores, A.; Marcos, M. Ocean swells along the global coastlines and their climate projections for the Twenty-First century. *J. Clim.* **2020**, *33*, 185–199. [CrossRef]
18. Sachini, P.; Ian, Y.; Alberto, M. Modelling swell propagation across the Pacific&#13. *Front. Mar. Sci.* **2023**, *10*, 1187473.
19. Merrifield, S.T.; Schramek, T.A.; Celona, S.; Bôas AB, V.; Colin, P.L.; Terrill, E.J. Typhoon-forced waves. *Oceanography* **2019**, *32*, 56–65. [CrossRef]
20. Liu, J.; Meucci, A.; Liu, Q.; Babanin, A.V.; Ierodiaconou, D.; Xu, X.; Young, I.R. A high-resolution wave energy assessment of south-east Australia based on a 40-year hindcast. *Renew. Energ.* **2023**, *215*, 118943. [CrossRef]
21. Li, R.; Wu, K.; Li, J.; Dong, X.; Sun, J.; Zhang, W.; Liu, Q. Relating a large-scale variation of waves in the indian ocean to the IOD. *J. Geophys. Res. Ocean.* **2022**, *127*, e2022JC018941. [CrossRef]
22. Li, R.; Wu, K.; Li, J.; Akhter, S.; Dong, X.; Sun, J.; Cao, T. Large-scale signals in the south pacific wave fields related to ENSO. *J. Geophys. Res. Ocean.* **2021**, *126*, e2021JC017643. [CrossRef]
23. Sasaki, W. Changes in the North Pacific wave climate since the mid-1990s. *Geophys. Res. Lett.* **2014**, *41*, 7854–7860. [CrossRef]
24. Mackay, E.B.L.; Retzler, C.H.; Challenor, P.G.; Gommenginger, C.P. A parametric model for ocean wave period from Ku band altimeter data. *J. Geophys. Res.* **2008**, *113*, 287–310.
25. Mcwilliams, J.C.; Restrepo, J.M. The Wave-Driven ocean circulation. *Am. Meteorol. Soc.* **1999**, *29*, 2523–2540. [CrossRef]
26. Zeng'An, D.; Kejian, W.; Dongliang, Z.; Ting, Y. Effects of wind waves of the Pacific westerly on the eastern Pacific wave transport. *Acta Oceanol. Sin.* **2009**, *1*, 83–88.
27. Zhang, J.; Wang, W.; Guan, C. Analysis of the global swell distributions using ECMWF Re-analyses wind wave data. *J. Ocean Univ. China* **2011**, *10*, 325–330. [CrossRef]
28. Gulev, S.K.G.V. Variability of the winter wind waves and swell in the north atlantic and north pacific as revealed by the voluntary observing ship data. *J. Clim.* **2006**, *19*, 5667–5685. [CrossRef]
29. Zheng, C.; Zhuang, H.; Li, X.; Li, X. Wind energy and wave energy resources assessment in the East China Sea and South China Sea. *Sci. China Technol. Sci.* **2012**, *55*, 163–173. [CrossRef]
30. Li, X.M. A new insight from space into swell propagation and crossing in the global oceans. *Geophys. Res. Lett.* **2016**, *43*, 5202–5209. [CrossRef]
31. Zhao, M.L.D. On the study of wave propagation and distribution in the global ocean. *J. Ocean Univ. China* **2019**, *18*, 803–811.
32. Pérez, J.; Méndez, F.J.; Menéndez, M.; Losada, I.J. ESTELA: A method for evaluating the source and travel time of the wave energy reaching a local area. *Ocean Dynam.* **2014**, *64*, 1181–1191. [CrossRef]
33. Hersbach, H.; Bell, B.; Berrisford, P.; Hirahara, S.; Horányi, A.; Sabater, J.M.; Nicolas, J.; Peubey, C.; Radu, R.; Schepers, D.; et al. The ERA5 global reanalysis. *Q. J. Roy. Meteor. Soc.* **2020**, *146*, 1999–2049. [CrossRef]
34. Sharmar, V.D.; Markina, M.Y.; Gulev, S.K. Global ocean wind-wave model hindcasts forced by different reanalyzes: A comparative assessment. *J. Geophys. Res. Ocean.* **2021**, *126*, e2020JC016710. [CrossRef]
35. Naseef, T.M.; Kumar, V.S. Climatology and trends of the Indian Ocean surface waves based on 39-year long ERA5 reanalysis data. *Int. J. Climatol.* **2020**, *40*, 979–1006. [CrossRef]
36. Sreelakshmi, S.; Bhaskaran, P.K. Regional wise characteristic study of significant wave height for the Indian Ocean. *Clim. Dynam.* **2020**, *54*, 3405–3423. [CrossRef]
37. Liu, Q.; Babanin, A.V.; Rogers, W.E.; Zieger, S.; Young, I.R.; Bidlot, J.R.; Durrant, T.; Ewans, K.; Guan, C.; Kirezci, C.; et al. Global wave hindcasts using the observation-based source terms: Description and validation. *J. Adv. Model. Earth Sy.* **2021**, *13*, e2021MS002493. [CrossRef]
38. Rascle, N.; Ardhuin, F. A global wave parameter database for geophysical applications. Part 2: Model validation with improved source term parameterization. *Ocean Model.* **2013**, *70*, 174–188. [CrossRef]
39. Echevarria, E.R.; Hemer, M.A.; Holbrook, N.J. Seasonal variability of the global spectral wind wave climate. *J. Geophys. Res. Ocean.* **2019**, *124*, 2924–2939. [CrossRef]
40. Munk, W.; Miller, G.; Snodgrass, F.; Barber, N. Directional recording of swell from distant storms. *Philos. Trans. R. Soc. A Math. Phys. Eng. Sci.* **1963**, *255*, 505–584, Erratum in *Philos. Trans. R. Society. Math. Phys. Eng. Sci.* **2013**, *371*, 20130039. [CrossRef]
41. Carrasco, A.; Semedo, A.; Isachsen, P.E.; Christensen, K.H.; Saetra, Ø. Global surface wave drift climate from ERA-40. *Ocean. dynamics* **2014**, *64*, 1815–1829. [CrossRef]
42. Wang, Y.; Liu, J.; Liu, H.; Lin, P.; Yuan, Y.; Chai, F. Seasonal and interannual variability in the sea surface temperature front in the eastern pacific ocean. *J. Geophys. Res. Ocean.* **2021**, *126*, e2020JC016356. [CrossRef]
43. Liu, J.; Wang, Y.; Yuan, Y.; Xu, D. The response of surface chlorophyll to mesoscale eddies generated in the eastern South China Sea. *J. Oceanogr.* **2020**, *76*, 211–226. [CrossRef]
44. Young, I.R.; Ribal, A. Multiplatform evaluation of global trends in wind speed and wave height. *Science* **2019**, *364*, 548–552. [CrossRef] [PubMed]